

Invariant-based inverse engineering for balanced displacement of a cart-pole system

I. Lizuain^{1,2}, A. Tobalina^{1,2}, and A. Rodriguez-Prieto^{1,2}

¹Department of Applied Mathematics, University of the Basque Country UPV/EHU, Bilbao 48013, Spain

²EHU Quantum Center, University of the Basque Country UPV/EHU, 48940 Leioa, Spain

Adiabaticity is a key concept in physics, but its applications in mechanical and control engineering remain underexplored. Adiabatic invariants ensure robust dynamics under slow changes, but they impose impractical time limitations. Shortcuts to Adiabaticity (STA) overcome these limitations by enabling fast operations with minimal final excitations. In this work, we set a STA strategy based on dynamical invariants and inverse engineering to design the trajectory of a cart-pole, a system characterized by its instability and repulsive potential. The trajectories found guarantee a balanced transport of the cart-pole within the small oscillations regime. The results are compared to numerical simulations with the exact non-linear model to set the working domain of the designed protocol.

1 Introduction

Underactuated systems, characterized by having fewer control inputs than degrees of freedom, are prevalent in a multitude of applications, ranging from robotics and aerospace to biomechanics [1]. These systems present significant control challenges due to inherent nonlinearities and limited actuation capabilities. Consequently, the development of effective control strategies for these systems, which are crucial for many economically relevant areas, has been an active field of research over the last decades.

The cart-pole system has become a widely recognized benchmark for evaluating control strategies for underactuated systems. This inverted pendulum setup, consisting of a pole hinged to a cart moving along a horizontal track (see Fig. 1), has been intensively studied in control theory because of its direct applications in various areas such as personal transport devices [2], robotic manipulators used in assembly lines [3] and humanoid robots, where the cart-pole model helps develop balancing algorithms [4]. Moreover, it is a usual benchmark for reinforcement learning algorithms [5] and neuromorphic computing [6]. Recently, the cart-pole model has even been extended to the quantum realm, where classical machine learning techniques have been used to balance the system. Here we take the same path but in the opposite direction. We apply control techniques originally developed for quantum systems to the classical cart-pole system.

The concept of adiabaticity is ubiquitous in physics, but it is not fully exploited in control engineering. Adiabatic theorems set the existence of approximate adiabatic invariants, such as the action integral in classical mechanics, when the control parameters vary slowly enough in time [7]. “Shortcuts To Adiabaticity” (STA) is a set of control methods developed to reach the same results of an adiabatic protocol in short times [8, 9]. Adiabaticity is often used to drive systems in a robust manner. An example is a load hanging

from an overhead crane. If the motion is slow enough, the energy of the pendulum is an adiabatic invariant and stays constant. In particular, if the load starts at the minimum energy configuration, this state is preserved throughout the operation [10, 11, 12]. STA accelerate the process and still achieve the same result, avoiding issues related to long operation times such as accumulation of random and/or uncontrollable perturbations.

STA methods have been successfully applied to a variety of control operations with quantum systems: quantum computation [13, 14, 15, 16], cooling [17, 18], quantum transport [19, 20], quantum state preparation [21, 22, 23, 24], manipulation of cold atoms [25, 26, 27, 28, 29, 30] or control of polyatomic molecules [31]. Perhaps surprisingly, because of the differing orders of magnitude involved, the dynamics of the cart-pole is closely related to that of a microscopic particle transport in moving traps [19, 32]. In both domains the linearized models imply the displacement of an inverted harmonic oscillator.

Cart pole control tasks usually correspond to either swing-up operations, where the pole goes from a downwards vertical position to the unstable equilibrium point at the vertical upwards position, or to balance operations, where the goal is to maintain the system at the upwards position. Here, besides aiming for balance, we consider a specific dynamical task, the displacement of the cart such that the cart-pole starts in the upwards vertical positions at certain location, and it finishes at a different position in the same balanced configuration. The design of the control operation is far from trivial since we will be dealing with a repulsive potential with unstable equilibrium [33]. Our STA approach is presented here without feedback but it may be combined with feedback control techniques.

The article is organized as follows. The physical model and Hamiltonian of the system are set in Sec. 2, both in exact form and in the small oscillation regime. In Sec. 3 dynamical invariants are identified and the STA protocol is designed. Numerical results are presented in Sec. 4 and, finally, in Sec. 5 we end with the conclusions and discuss some open questions.

2 Physical model and basic equations

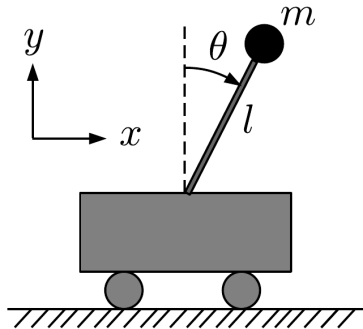


Figure 1: Inverted pendulum on a cartpole. Physical model and relevant parameters.

The physical model and relevant parameters are shown in Fig. 1. The model assumes several conditions and idealizations: (i) the mass of the wires and friction are neglected; (ii) point masses; (iii) constant wire lengths l ; (iv) the cartpole position is treated as a control parameter rather than a dynamical variable. This last assumption is a common simplification [34], often used to facilitate control design, but it requires a well-designed controller to ensure accurate implementation. A more fundamental approach, where the cartpole position is treated as a dynamical variable, is also possible and would allow for a more detailed analysis of energy consumption of STA protocols as explored in [10].

In terms of the generalized angle θ , the position of the load is given by its cartesian coordinates

$$x(t) = x_0(t) + l \sin \theta(t) ; y(t) = l \cos \theta(t) \quad (1)$$

where the cartpole's position $x_0(t)$ is the control parameter to be engineered. The kinetic (T) and potential (V) are written as

$$T = \frac{1}{2}m(\dot{x}^2 + \dot{y}^2); \quad V = mgy, \quad (2)$$

where dots represent time derivatives and where we have dropped the explicit time dependence from the variables for simplicity. The Lagrangian of the system can then be written as $\mathcal{L} = T - V$, from where the equation of motion of the load can be easily derived from Euler-Lagrange equations $\frac{d}{dt} \frac{\partial \mathcal{L}}{\partial \dot{\theta}} - \frac{\partial \mathcal{L}}{\partial \theta} = 0$,

$$l\ddot{\theta} - g \sin \theta = -\ddot{x}_0 \cos \theta. \quad (3)$$

Using now the horizontal displacement of the mass $q = \sin \theta$ as the new variable and assuming small oscillations, the dynamics of the system is described, to first order in θ , by the linear equation

$$\ddot{q} - \omega^2 q = -\ddot{x}_0 \quad (4)$$

which corresponds to a forced inverted harmonic oscillator with natural frequency $\omega^2 = g/l$. It is easy to show that this equation of motion may also be derived from the Hamiltonian

$$H = \frac{p^2}{2m} - \frac{1}{2}m\omega^2 q^2 + m\dot{x}_0 q, \quad (5)$$

where in this small oscillation regime $p = m\dot{q}$. This approximation linearizes the dynamical equations of motion of the system. Results found with exact and approximate dynamics will be compared later to check the validity of the approximation and its limits.

3 Shortcuts to adiabaticity

3.1 Dynamical invariant

A dynamical invariant of a Hamiltonian system remains constant during the time evolution [35]. If I is an invariant of H , the following equation is satisfied,

$$\frac{dI}{dt} = \partial_t I + \{I, H\} = 0, \quad (6)$$

where $\{I, H\}$ refers to the Poisson bracket. Quadratic Hamiltonians with a linear in position term, form the so-called Lewis-Leach family of Hamiltonians whose quadratic invariants are explicitly known [36]. The invariant I of the Hamiltonian of our particular system needs some minor modifications from the Lewis-Leach invariants [36, 9] due to the repulsive behaviour of the potential involved. In particular, let us take the following expression for I ,

$$I = \frac{1}{2m}(p - m\dot{\alpha})^2 - \frac{1}{2}m\omega^2(q - \alpha)^2, \quad (7)$$

whose time derivative

$$\frac{dI}{dt} = \partial_t I + \frac{\partial H}{\partial p} \frac{\partial I}{\partial q} - \frac{\partial H}{\partial q} \frac{\partial I}{\partial p} = (m\dot{\alpha} - p) (\ddot{\alpha} - \omega^2 \alpha + \ddot{x}_0) \quad (8)$$

will be identically zero as long as the function $\alpha(t)$ satisfies the auxiliary equation

$$\ddot{\alpha} - \omega^2 \alpha = -\ddot{x}_0. \quad (9)$$

Therefore, if $\alpha(t)$ satisfies above equation, I , as defined in Eq. (7), will be a dynamical invariant of the Hamiltonian (5) and will remain constant during the time evolution of the system. This auxiliary equation (9) is the Newton equation of motion for a forced harmonic (and inverted) oscillator. This α function may be regarded as an auxiliary function satisfying the same Newton equation (4). However, we shall impose to α some extra boundary conditions that will guarantee zero final excitations as we shall see.

3.2 Shortcut to adiabaticity

Let us now impose the following boundary conditions (BC) for the auxiliary equation just derived:

$$\alpha(t_b) = \dot{\alpha}(t_b) = \ddot{\alpha}(t_b) = 0. \quad (10)$$

where $t_b = 0, t_f$ stands for *boundary* times. These boundary conditions guarantee that the invariant I in Eq. (7) coincides with the Hamiltonian H at initial and final times. Moreover, at boundary times, the imposed BCs also imply that $\ddot{x}(t_b) = 0$ so that the Hamiltonian represents the total mechanical energy of the system. Therefore, if the above BCs are satisfied, the invariant I , Hamiltonian H and total mechanical energy E will coincide at boundary times, $I(t_b) = H(t_b) = E(t_b)$. Then, if a fast finite-time process is designed so that the auxiliary function α satisfy boundary conditions in (10), the energy at initial and final times will coincide regardless of the initial conditions since

$$E(0) = H(0) = I(0) = I(t_f) = H(t_f) = E(t_f). \quad (11)$$

In the following, we will show how to construct the cartpole trajectory $x_0(t)$, by means of an inverse engineering approach, so that the desired conditions in (10) are satisfied.

3.3 Inverse engineering

The inverse engineering strategy is relatively simple. From (9) and integrating twice with respect to time we may write the cartpole trajectory as

$$x_0(t) = \int_0^t \int_0^{\tau_2} [\omega^2 \alpha(\tau_1) - \ddot{\alpha}(\tau_1)] d\tau_1 d\tau_2. \quad (12)$$

This function should also obey some physical boundary conditions. In particular, we must impose at final time that

$$x_0(t_f) = d ; \dot{x}_0(t_f) = 0 \quad (13)$$

i. e., the transported distance and the final time smooth operation. There are, in summary, eight boundary conditions to be satisfied: the six conditions for $\alpha(t)$ given in (10), plus these final times conditions (13). Note that the conditions at initial times $x_0(0) = \dot{x}_0(0) = 0$ do not have to be imposed, since they are automatically satisfied by construction.

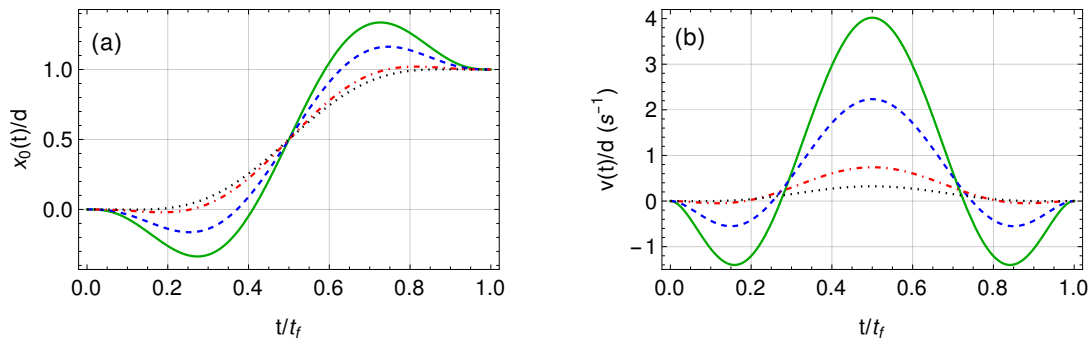


Figure 2: (Color online) Cartpole trajectories (a) and velocities (b) for different total process time t_f . $t_f = 1.5$ s green-solid, $t_f = 2$ s dashed-blue, $t_f = 4$ s red dashed-dotted and $t_f = 8$ s black dotted. Other parameters: $l = 1$ m.

We adopt a seventh-degree polynomial ansatz for the auxiliary function α :

$$\alpha(t) = \sum_{k=0}^7 a_k \tau^k \quad (14)$$

where $\tau = t/t_f$. The eight free parameters a_k will be determined by imposing the corresponding boundary conditions. This ansatz is one possible choice among many functional forms. However, we select this polynomial ansatz for its simplicity, favorable mathematical properties (such as smoothness and ease of differentiation) and its flexibility in efficiently satisfying boundary conditions.

Parameters a_0, \dots, a_5 are obtained imposing (10), while the remaining a_6, a_7 are obtained imposing (13). This leads to the following cartpole trajectory,

$$x_0(t) = d \left[126\tau^5 - 420\tau^6 + 540\tau^7 - 315\tau^8 + 70\tau^9 + \frac{1}{\omega^2 t_f^2} \left(-2520\tau^3 + 12600\tau^4 - 22680\tau^5 + 17640\tau^6 - 5040\tau^7 \right) \right] \quad (15)$$

see some cartpole trajectories and velocities in Fig. 2. For short times, the velocities and accelerations involved in the process are quite large as expected, and there are several segments of braking and acceleration. On the other hand, for slow processes ($\omega t_f \gg 1$), the second term in (15) vanishes and the trajectory $x_0(t)$ tends asymptotically to

$$x_\infty(t) = d \left(126\tau^5 - 420\tau^6 + 540\tau^7 - 315\tau^8 + 70\tau^9 \right). \quad (16)$$

In this regime, there is only one acceleration time segment up to $t_f/2$ (inflexion point of x_∞) and a subsequent braking segment. The maximal velocity reached by the cartpole in this asymptotic scenario is $\dot{x}_\infty(t_f/2) = \frac{315}{128} \left(\frac{d}{t_f} \right)$.

4 Numerical Results

Once the trajectory for the cartpole has been designed, the dynamical equation of motion can be integrated either numerically in its *exact* form (3) or analytically in its approximated, harmonic linearized version (4). See some results in Fig. 3.

It is important to underline that the designed shortcut protocol will work as long as the small oscillation regime holds, i. e., as long as the swing angle θ is small throughout

the transport process. We shall only consider the case where the cartpole is initially in equilibrium (null initial conditions), since this is the most interesting scenario. In this situation, a *perfect* shortcut should lead to the same final configuration (pendulum in equilibrium). This is indeed what happens if the linear equation of motion is integrated (red-dashed lines in Fig. 3). In the exact case however, deviations from the target final configuration are observed (blue solid lines in Fig. 3). For large transport distances d , short pendulum lengths l or short process times t_f , anharmonic effects become more and more important, deviating from the ideal result and limiting the validity of our shortcut protocol. We study these non-linear effects in detail in the following sub-section.

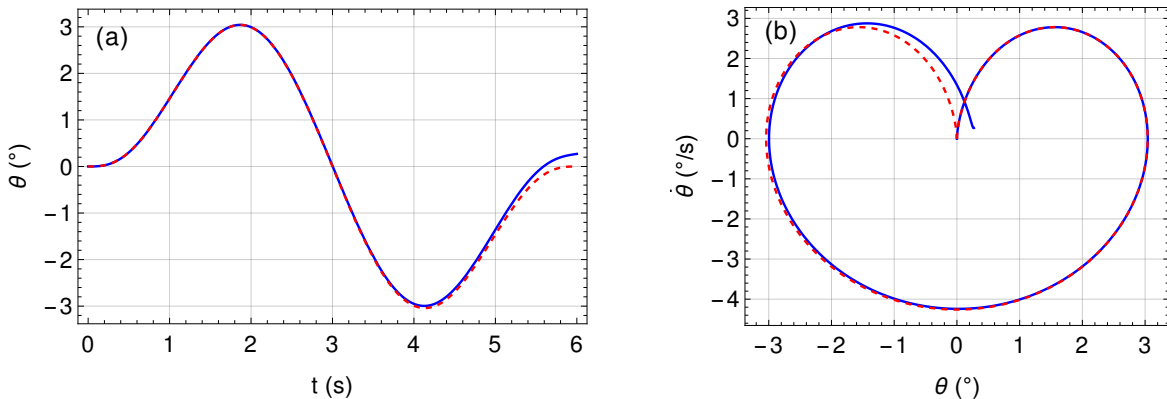


Figure 3: (Color online) (a) Cartpole swing angle θ as a function of time after numerically integrating the exact dynamical equation (3) (blue solid line) and linearized harmonic model (4) (red dashed line). with null initial conditions $\theta(0) = \dot{\theta}(0) = 0$. (b) Phase-space diagram for the same process. Linearized model leads to purely periodic motion and therefore closed orbits in phase-space, whereas nonlinearities of the exact, more realistic and complex model, lead to deviations in the ideal target configuration at final time. Other parameters: $l = 10\text{m}$, $d = 2\text{m}$, $t_f = 6\text{s}$.

4.1 Non-linear effects

Let us start by looking at the contribution that the different physical parameters have on the the non-linear effects in the dynamical equation (3) when the cartpole trajectory given by (15). The role of the transport distance d and pendulum length l is clear. Larger distances d imply larger accelerations so an increase of anharmonic effects is expected and, a larger pendulum, implies a *flatter* potential so the non-linear effects would decrease as l increases.

The effect of the transport total time t_f is not that clear at first sight. This quantify enters the differential equation as a parameter via the cartpole's acceleration term on the right hand side of (3). It is then clear that longer processes would imply lower accelerations, so that non-linear effects would decrease as t_f increase. But, on the other hand, t_f also enters the dynamical equation as the final integration limit. Therefore, long processes would also imply an increase of the anharmonic effects since for longer integration times these effects would start to accumulate, leading to undesired final tiempo excitations.

This is more clearly visualized if we write (3) using a dimensionless time $\tau = t/t_f$ as a parameter. The equation of motion (that should be now integrated from $\tau = 0$ to $\tau = 1$) takes the dimensionless form

$$\ddot{\theta} = \frac{gt_f^2}{l} \sin \theta - \frac{d}{l} a_1 \cos \theta - \frac{d}{gt_f^2} a_2 \cos \theta, \quad (17)$$

where dots now represent derivatives with respect to τ and $a_{1,2}$ are different terms of a *dimensionless* acceleration

$$a_1(\tau) = 5040\tau^7 - 17640\tau^6 + 22680\tau^5 - 12600\tau^4 + 2520\tau^3 \quad (18)$$

$$a_2(\tau) = -211680\tau^5 + 529200\tau^4 - 453600\tau^3 + 151200\tau^2 - 15120\tau. \quad (19)$$

The effect of each parameter is now clear: larger d or smaller l implies larger non-linear effects, whereas the effect of t_f is twofold, so a compromise in this magnitude would be needed.

To quantify the excitation at final time in a way that is easy to understand and visualize, we measure the final energy ΔE in terms of a *fictitious* angle Θ . This angle is defined as the final angle when the final energy is considered (artificially) to be purely potential. This angle is a way to measure the final excitation energy in terms of a more visual quantity. Taking the pendulum vertical position as the zero of the potential energy and considering null initial conditions (pendulum initially in equilibrium), the initial energy is $E(0) = 0$, so the energy difference is given by

$$\Delta E = E(t_f) - E(0) = \frac{1}{2}ml^2\dot{\theta}(t_f)^2 + 2mgl \sin^2 \frac{\theta(t_f)}{2}, \quad (20)$$

where the values of θ and $\dot{\theta}$ at $t = t_f$ are obtained by numerically integrating (3). This final energy has contributions from both kinetic and potential energies. One can artificially consider this final energy to be purely potential by defining the fictitious angle Θ by the relation $\Delta E = 2mgl \sin^2 \frac{\Theta}{2}$ so that

$$\Theta = 2 \arcsin \left[\sqrt{\frac{l\dot{\theta}(t_f)^2}{4g} + \sin^2 \frac{\theta(t_f)}{2}} \right]. \quad (21)$$

Some results of this quantity are shown in Fig. 4 in different scenarios. As previously commented, for a given configuration of transport distance d and pendulum length l , too short or too long processes lead to undesired final excitations. One can also numerically obtain the optimal value of each process time t_f so that the resultant fictitious angle Θ is minimal for a given d - l configuration (minima of each curve in Fig. 4), see some results and comments in Fig. 5.

5 Conclusions

In this work, an invariant based inverse engineering STA method has been applied to control the transport of a mass on an inverted pendulum cartpole, a mechanical system characterized by its instability and repulsive potential. The designed transport protocol minimizes final energy excitations without requiring feedback. Numerical simulations using the exact non-linear model allows us to check the parameter interval where the protocol is accurate and works properly, and also allows us to quantify the final excitations due to its inherent non-linear behaviour. These simulations validate the effectiveness of our approach, demonstrating its potential for practical applications in robotics and automation.

The results highlight the advantages of STA methods in overcoming the limitations of adiabatic processes, which, while robust, impose impractically long operation times. The inverse engineering approach allows us to generate trajectories that achieve fast and minimal excitation transport, expanding the applicability of STA beyond quantum and microscopic systems to classical mechanical engineering problems.

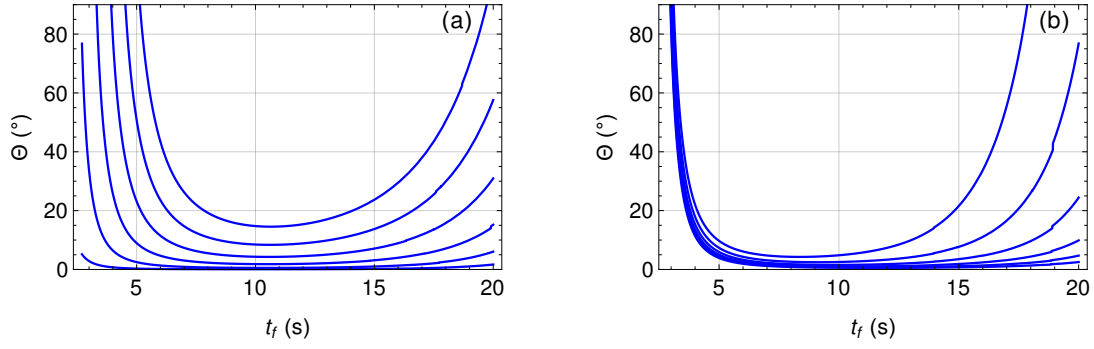


Figure 4: (Color online) Fictitious angle Θ as a function of the process time t_f in different scenarios. As discussed in the text, this angle quantifies the final deviation from the ideal balanced final state. Numerical results clearly indicate that both excessively fast or slow processes result in undesirably high final angle configurations, whereas an optimal time window minimizes final excitation. Outside this optimal region, nonlinear effects become increasingly significant, causing the protocol to break down and leading to final configurations with very large angles. (a) From bottom to top $d = 2, 4, 6, 8, 10, 12$ m for a fixed pendulum length of $l = 16$ m. (b) From bottom to top $l = 10, 12, 14, 16, 18, 20$ m for fixed value of $d = 5$ m. Pendulum initially in equilibrium.

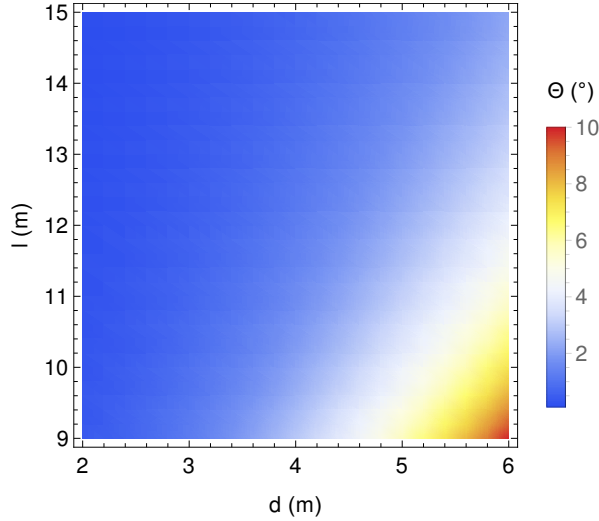


Figure 5: (Color online) Minimum of final time excitations measured by the value of the fictitious angle Θ (in $^\circ$) as a function of d and l . For each d - l configuration, the optimal process time t_f is numerically calculated as the minimum of each curve in Fig. 4. Using this optimal time, the possible minimum fictitious angle is computed for that particular configuration. In other words, this plot illustrates the best-case scenario for a given d - l configuration. For larger values of d or smaller values of l , final excitations larger than 10° are obtained.

One of the key features of the STA approach we have followed is its flexibility. It should be underlined that we have not really optimized the trajectory. We have inverse engineered the trajectory by means of a polynomial ansatz, but of course this choice, and therefore the solutions to the inverse problem are not unique, leaving room for further optimization based on specific performance criteria, such as robustness to different kind of perturbations and/or energy cost and efficiency.

Although this work focuses on non-feedback control, hybrid control strategies combining STA with some feedback mechanism is an interesting open line for future research. Future

work could also explore the extension of this protocol to more complex systems such as dynamical systems with higher degrees of freedom (double or triple pendulums). These extensions would further improve the robustness of the method to real-world industrial and robotic applications.

Acknowledgments

This research was funded by the Basque Government through Grant No. IT1470-22 and Spanish Government MCIU through Grant No. PID2021-126273NB-I00.

References

- [1] Mark W. Spong. Underactuated mechanical systems. In Bruno Siciliano and Kimon P. Valavanis, editors, *Control Problems in Robotics and Automation*, pages 135–150. Springer Berlin Heidelberg, 1998.
- [2] Mostafa Nikpour, Loulin Huang, and Ahmed M. Al-Jumaily. Stability and direction control of a two-wheeled robotic wheelchair through a movable mechanism. *IEEE Access*, 8:45221–45230, 2020.
- [3] B. Siciliano and O. Khatib. *Springer Handbook of Robotics*. Springer Cham, 2016.
- [4] Qiang Huang, K. Yokoi, S. Kajita, K. Kaneko, H. Arai, N. Koyachi, and K. Tanie. Planning walking patterns for a biped robot. *IEEE Transactions on Robotics and Automation*, 17(3):280–289, 2001.
- [5] Zhikang T. Wang, Yuto Ashida, and Masahito Ueda. Deep reinforcement learning control of quantum cartpoles. *Phys. Rev. Lett.*, 125:100401, Sep 2020.
- [6] James S. Plank, Charles P. Rizzo, Chris A. White, and Catherine D. Schuman. The cart-pole application as a benchmark for neuromorphic computing. *Journal of Low Power Electronics and Applications*, 15(1), 2025.
- [7] J. J. Sakurai. *Modern Quantum Mechanics; rev. ed.* Adison-Wesley, Reading, MA, 1994.
- [8] Erik Torrontegui, Sara Ibáñez, Sofia Martínez-Garaot, Michele Modugno, Adolfo del Campo, David Guéry-Odelin, Andreas Ruschhaupt, Xi Chen, and Juan Gonzalo Muga. Shortcuts to adiabaticity. *Advances In Atomic, Molecular, and Optical Physics*, 62:117 – 169, 2013.
- [9] D. Guéry-Odelin, A. Ruschhaupt, A. Kiely, E. Torrontegui, S. Martínez-Garaot, and J. G. Muga. Shortcuts to adiabaticity: Concepts, methods, and applications. *Rev. Mod. Phys.*, 91:045001, Oct 2019.
- [10] E. Torrontegui, I. Lizuain, S. González-Resines, A. Tobalina, A. Ruschhaupt, R. Kosloff, and J. G. Muga. Energy consumption for shortcuts to adiabaticity. *Phys. Rev. A*, 96:022133, 2017.
- [11] S. González-Resines, D. Guéry-Odelin, A. Tobalina, I. Lizuain, E. Torrontegui, and J. G. Muga. Invariant-based inverse engineering of crane control parameters. *Phys. Rev. Applied*, 8:054008, 2017.
- [12] Ion Lizuain, Ander Tobalina, Alvaro Rodriguez-Prieto, and Juan Gonzalo Muga. Invariant-based inverse engineering for fast and robust load transport in a double pendulum bridge crane. *Entropy*, 22(3), 2020.
- [13] M.S. Sarandy, E.I. Duzzioni, and R.M. Serrac. Quantum computation in continuous time using dynamic invariants. *Phys. Lett. A*, 375:3343–3347, 2011.
- [14] M. Palmero, S. Martínez-Garaot, D. Leibfried, D. J. Wineland, and J.G. Muga. Fast phase gates with trapped ions. *Phys. Rev. A*, 95:022328, 2017.

- [15] A. del Campo, M. M. Rams, and W. H. Zurek. Assisted finite-rate adiabatic passage across a quantum critical point: Exact solution for the quantum ising model. *Phys. Rev. Lett.*, 109:115703, 2012.
- [16] K. Takahashi. Shortcuts to adiabaticity for quantum annealing. *Phys. Rev. A*, 95:012309, 2017.
- [17] R. Onofrio. Physics of our days: Cooling and thermometry of atomic fermi gases. *Phys.-Usp.*, 59:1129, 2017.
- [18] Roie Dann, Ander Tobalina, and Ronnie Kosloff. Fast route to equilibration. *Phys. Rev. A*, 101:052102, May 2020.
- [19] E. Torrontegui, S. Ibáñez, X. Chen, A. Ruschhaupt, D. Guéry-Odelin, and J. G. Muga. Fast atomic transport without vibrational heating. *Phys. Rev. A*, 83:013415, 2011.
- [20] R. Bowler, J. Gaebler, Y. Lin, T. R. Tan, D. Hanneke, J. D. Jost, D. Home, J. P. Leibfried, and D. J. Wineland. Coherent diabatic ion transport and separation in a multizone trap array. *Phys. Rev. Lett.*, 109:080502, 2012.
- [21] X. Chen, I. Lizuain, A. Ruschhaupt, D. Guéry-Odelin, and J. G. Muga. Shortcut to adiabatic passage in two- and three-level atoms. *Phys. Rev. Lett.*, 105:123003, 2010.
- [22] M. G. Bason, M. Viteau, N. Malossi, P. Huillery, E. Arimondo, D. Ciampini, R. Fazio, V. Giovannetti, R. Manella, and O. Morsch. High-fidelity quantum driving. *Nat. Phys.*, 8:147–152, 2012.
- [23] J. Zhang, J. H. Shim, I. Niemeyer, T. Taniguchi, T. Teraji, H. Abe, S. Onoda, T. Yamamoto, T. Ohshima, J. Isoya, and D. Suter. Experimental implementation of assisted quantum adiabatic passage in a single spin. *Phys. Rev. Lett.*, 110:240501, 2013.
- [24] B. B. Zhou, A. Baksic, H. Ribeiro, C. G. Yale, F. J. Heremans, P. C. Jerger, A. Auer, G. Burkard, Clerk A. A., and D. D. Awschalom. Accelerated quantum control using superadiabatic dynamics in a solid-state lambda system. *Nat. Phys.*, 13:330–334, 2017.
- [25] E. Torrontegui, X. Chen, M. Modugno, S. Schmidt, A. Ruschhaupt, and J. G. Muga. Fast transport of bose–einstein condensates. *New J. Phys.*, 14:013031, 2012.
- [26] W. Rohringer, D. Fischer, F. Steiner, I. E. Mazets, J. Schmiedmayer, and M. Trupke. Non-equilibrium scale invariance and shortcuts to adiabaticity in a one-dimensional bose gas. *Sci. Rep.*, 5:9820, 2015.
- [27] J. F. Schaff, X. L. Song, P. Vignolo, and G. Labeyrie. Fast optimal transition between two equilibrium states. *Phys. Rev. A*, 82:033430, 2010.
- [28] J. F. Schaff, P. Capuzzi, G. Labeyrie, and P. Vignolo. Shortcuts to adiabaticity for trapped ultracold gases. *New J. Phys.*, 13:113017, 2011.
- [29] E. Torrontegui, S. Martinez-Garaot, M. Modugno, X. Chen, and J. G. Muga. Engineering fast and stable splitting of matter waves. *Phys. Rev. A*, 87:033630, 2013.
- [30] A. Kiely, A. Benseny, T. Busch, and A. Ruschhaupt. Shaken not stirred: creating exotic angular momentum states by shaking an optical lattice. *J. Phys. B: At. Mol. Opt. Phys.*, 49(21):215003, 2013.
- [31] S. Mashuda and S. A. Rice. Fast-forward assisted stirap. *J. Phys. Chem. A*, 119:3479–3487, 2015.
- [32] S. Martínez-Garaot A. Tobalina, M. Palmero and J. G. Muga. Fast atom transport and launching in a nonrigid trap. *Scientific Reports*, 7:5753, July 2017.
- [33] Lanlan Ma and Qian Kong. Optimal shortcuts to adiabatic control by lagrange mechanics. *Entropy*, 25(5), 2023.
- [34] Eihab M. Abdel-Rahman, Ali H. Nayfeh, and Ziyad N. Masoud. Dynamics and control of cranes: A review. *Modal Analysis*, 9(7):863–908, jul 2003.

- [35] T. Damour, P. Jaranowski, and G. Schäfer. Dynamical invariants for general relativistic two-body systems at the third post-newtonian approximation. *Phys. Rev. D.*, 62:044024, 2000.
- [36] H. R. Lewis and P. G. L. Leach. Exact invariants for a class of time-dependent non-linear hamiltonian-systems. *J. Math. Phys.*, 23(1):165–175, 1982.